



Article

Direct Torque Control of Dual Three-Phase Permanent Magnet Synchronous Motors Based on Master–Slave Virtual Vectors

Qiang Geng ¹, Ziteng Qin ¹, Xuefeng Jin ¹, Guozheng Zhang ¹ and Zhanqing Zhou ^{2,*}

¹ Tianjin Key Laboratory of Intelligent Control of Electrical Equipment, Tiangong University, Tianjin 300387, China; gengqiang@tju.edu.cn (Q.G.); 2131070894@tiangong.edu.cn (Z.Q.); jinxuefeng@tiangong.edu.cn (X.J.); zhanggz@tju.edu.cn (G.Z.)

² Advanced Electrical Equipment Innovation Center, Zhejiang University, Hangzhou 311107, China

* Correspondence: zhouzhanqing@tiangong.edu.cn

Abstract: In order to further reduce the torque, flux-linkage fluctuation, and current harmonic content of dual three-phase permanent magnet synchronous motors, this paper proposes a direct torque control strategy combined with a master–slave virtual vector duty cycle assignment. Two types of virtual voltage vectors with different amplitudes are used to form a harmonic suppression switching table. The virtual vectors are classified into master and slave virtual vectors according to the degree of influence on the torque and the flux-linkage. Then, the duty cycle of the master and slave virtual vectors is recalculated and allocated through the evaluation function to achieve accurate control of the torque and the flux-linkage. Finally, the switching sequences of the master and slave virtual vectors that act together in one control cycle are rearranged into a symmetrical waveform. It is experimentally verified that the phase current THD of the proposed strategy is reduced by 69.4%, the 5th and 7th current harmonics content is significantly reduced, and the torque fluctuation and flux-linkage fluctuation can also be effectively suppressed, which provides better dynamic performance and steady-state performance.

Keywords: dual three-phase permanent magnet synchronous motor; direct torque control; master–slave virtual vectors; duty cycle distribution; switch sequence correction



Citation: Geng, Q.; Qin, Z.; Jin, X.; Zhang, G.; Zhou, Z. Direct Torque Control of Dual Three-Phase Permanent Magnet Synchronous Motors Based on Master–Slave Virtual Vectors. *World Electr. Veh. J.* **2024**, *15*, 199. <https://doi.org/10.3390/wevj15050199>

Academic Editor: Paulo J. G. Pereira

Received: 18 March 2024

Revised: 26 April 2024

Accepted: 1 May 2024

Published: 4 May 2024



Copyright: © 2024 by the authors. Licensee MDPI, Basel, Switzerland. This article is an open access article distributed under the terms and conditions of the Creative Commons Attribution (CC BY) license (<https://creativecommons.org/licenses/by/4.0/>).

1. Introduction

With the increasing demand for the power and safety of motor systems in engineering applications such as aerospace and electric vehicles, the research on multiphase motors with high power and high reliability has attained significant proportions in recent years. Among various multiphase drives, the dual three-phase permanent magnet synchronous motor (DTP-PMSM) drives have the advantages of both multiphase motor drives and permanent magnet motor drives. Compared to three-phase drives, the DTP-PMSM drives offer superior features of reduced torque ripple and remarkable fault tolerance capability [1–3].

The direct torque control (DTC) scheme has a simpler structure and faster dynamic response in comparison with field-oriented control (FOC). Meanwhile, for DTP-PMSMs, the six-phase inverter that drives the motor operation can generate more voltage vectors, which provides a rich vector control set for the DTC scheme and enhances the flexibility of the control strategy, but also increases the difficulty of the algorithm design [4,5]. In addition, it is noted that only closed-loop control of the fundamental subspace will cause a larger harmonic current due to the relatively small impedance of harmonic subspace in the mathematical model of vector space decomposition (VSD) [6,7].

The voltage vectors controlling the DTP-PMSM drives contain 60 effective vectors and 4 zero vectors, which can be divided into four groups according to the magnitude of the vectors. So as to decrease the complexity of the switching table and increase the voltage utilization, the traditional DTC switching table of DTP-PMSMs only selects the

12 large vectors with the largest magnitude on the fundamental subspace. For the sake of solving the problem of current harmonics in a large vector-based DTC scheme, the modified intermediate vectors are applied to suppress the 5th and 7th harmonics in the harmonic subspace. The modified vector was centralized for simplifying the hardware implementation [8]. In some of the literature [9–12], the non-harmonic voltage vector switching table is applied to reduce the current harmonics. Moreover, the high-order torque hysteresis controller is used to divide the hysteresis width into several adjustment intervals, which can suppress the torque fluctuation and steady-state error, but the voltage utilization of this strategy will be reduced to a certain extent. To suppress the torque fluctuation of the DTC of DTP-PMSMs, some scholars have proposed vector space modulation technology. Scholars propose a direct torque control strategy of DTP-PMSMs based on vector space modulation, which not only reduces harmonic current and torque fluctuation but also ensures constant switching frequency [13]. In [14], a hybrid DTC strategy suitable for DTP-PMSMs is proposed. The strategy adopts different torque control modes in dynamic and steady-state modes, respectively, and an observer is designed to realize the tracking control of the flux-linkage. Some scholars also combine DTC with model predictive control (MPC) to reduce the predicted voltage vectors [15,16]. In [17], based on 36 effective vectors, the two-step table lookup method is proposed to reduce the calculated vectors. Firstly, 13 vectors are screened out in the fundamental subspace by the positive and negative of the torque error, and then the vectors are further reduced according to the principle of reducing the flux of the harmonic subspace, which simplifies the computational process. In [18], an enhanced DTC strategy based on discrete virtual vectors is proposed to improve the steady-state performance of PMSMs. The proposed strategy maintains the simple control structure and ideal dynamic performance of the DTC strategy and improves the steady-state performance by reducing torque ripple and current distortion. The experiment verifies the effectiveness of the proposed DTC strategy. In [19], the article considers the potential voltage imbalance in the DC link between two DC voltage source inverters of DTP-PMSMs. In order to solve these problems, a DTC strategy considering unbalanced DC side voltage is proposed in this study to improve the performance of DTP-PMSMs using virtual vectors.

Compared with vector control strategies, traditional DTC control saves the complicated coordinate transformation, and can realize the fast response adjustment of the motor by controlling the torque. This method is simple in structure and is not sensitive to the parameters of the motor and external influences. However, in order to ensure the fast dynamic performance of the motor torque, the large vectors are selected for voltage synthesis. The large vector of the α - β subspace will generate a large harmonic current in the harmonic subspace, so the traditional DTC control strategy will have some problems such as a large torque ripple.

Aiming to address the limitations of traditional DTC control for DTP-PMSM drives, a master–slave virtual vector direct torque control strategy based on duty cycle allocation is put forward in this paper to enhance the accuracy of torque/flux-linkage control accuracy and suppress current harmonics. Firstly, different methods are employed to synthesize the virtual vector to suppress current harmonics under various motor operating conditions. Then, considering the impact of torque and flux-linkage, the synthesized virtual vector is divided into master and slave virtual vectors. The duty cycle of each virtual vector is calculated and redistributed based on specific deviations in torque and flux-linkage, enabling precise control over both parameters. Finally, the switch sequence generated by the master and slave virtual vectors is modified to achieve a symmetrical waveform output for motor control. The simulation and experimental results show that compared with the traditional DTC control strategy, the proposed strategy can not only effectively suppress the flux-linkage and torque ripple under different operating conditions but also reduce the difficulty of hardware implementation and ensure the effectiveness of harmonic suppression through the reallocation of the master–slave virtual vector duty cycle.

2. Mathematical Model of Dual Three-Phase PMSMs

The stator of a DTP-PMSM consists of two sets of Y-connected three-phase symmetrical winding, which are spatially separated by an electrical angle of 30° and are driven by a six-phase voltage source inverter, as shown in Figure 1.

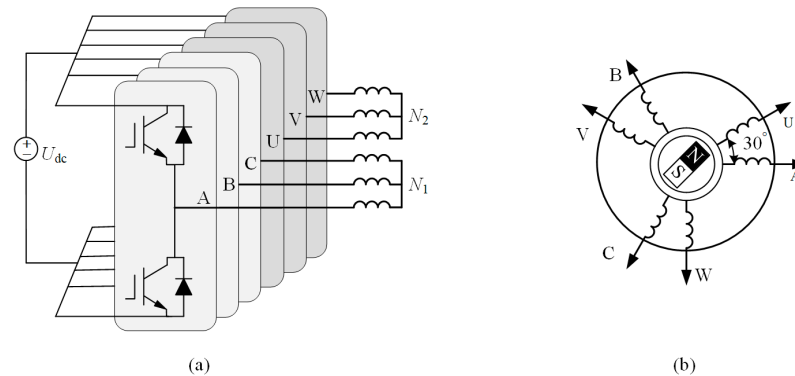


Figure 1. Dual three-phase PMSM drive system diagram: (a) six-phase inverter; (b) dual three-phase PMSM.

The static coordinate transformation matrix of DTP-PMSMs is shown in (1).

$$T_{6s/2s} = \frac{1}{3} \begin{bmatrix} 1 & -\frac{1}{2} & -\frac{1}{2} & \frac{\sqrt{3}}{2} & -\frac{\sqrt{3}}{2} & 0 \\ 0 & \frac{\sqrt{3}}{2} & -\frac{\sqrt{3}}{2} & \frac{1}{2} & \frac{1}{2} & -1 \\ 1 & -\frac{1}{2} & -\frac{1}{2} & -\frac{\sqrt{3}}{2} & \frac{\sqrt{3}}{2} & 0 \\ 0 & -\frac{\sqrt{3}}{2} & \frac{\sqrt{3}}{2} & \frac{1}{2} & \frac{1}{2} & -1 \\ 1 & 1 & 1 & 0 & 0 & 0 \\ 0 & 0 & 0 & 1 & 1 & 1 \end{bmatrix} \quad (1)$$

According to the VSD theory, the mathematical model in the static coordinate system of DTP-PMSMs can be decoupled into three two-dimensional orthogonal subspaces, respectively, α - β , x - y , and o_1 - o_2 . The components on the α - β subspace comprise the fundamental and harmonic components with orders of $12m \pm 1$ ($m = 1, 3, 5, \dots$), which are related to torque generation. The components on the x - y subspace comprise the harmonic components with orders of $6m \pm 1$ ($m = 1, 3, 5, \dots$), which do not participate in torque generation. The components on the o_1 - o_2 subspace are the zero-sequence components, which comprise the harmonic components with orders of $6m \pm 3$ ($m = 1, 3, 5, \dots$).

The transformation matrix of the rotating coordinate system of DTP-PMSMs is shown in (2).

$$T_{s/r} = \begin{bmatrix} \cos \theta & \sin \theta & 0 \\ -\sin \theta & \cos \theta & 0 \\ 0 & 0 & I_A \end{bmatrix} \quad (2)$$

When the neutral points of the two winding sets are isolated from each other, the zero-sequence subspace can be ignored, then the voltage and torque equations in the rotating coordinate system are as follows, respectively:

$$\begin{bmatrix} u_d \\ u_q \end{bmatrix} = \begin{bmatrix} R_s & \omega L_q \\ \omega L_d & R_s \end{bmatrix} \begin{bmatrix} i_d \\ i_q \end{bmatrix} + \begin{bmatrix} L_d \\ L_q \end{bmatrix} \begin{bmatrix} n_p i_d \\ n_p i_q \end{bmatrix} + \begin{bmatrix} 0 \\ \omega \psi_s \end{bmatrix} \quad (3)$$

$$\begin{bmatrix} u_x \\ u_y \end{bmatrix} = \begin{bmatrix} R_s & 0 \\ 0 & R_s \end{bmatrix} \begin{bmatrix} i_x \\ i_y \end{bmatrix} + L_z \begin{bmatrix} n_p i_x \\ n_p i_y \end{bmatrix} \quad (4)$$

$$\begin{bmatrix} \psi_d \\ \psi_q \\ \psi_x \\ \psi_y \end{bmatrix} = \begin{bmatrix} L_d & 0 & 0 & 0 \\ 0 & L_q & 0 & 0 \\ 0 & 0 & L_z & 0 \\ 0 & 0 & 0 & L_z \end{bmatrix} \begin{bmatrix} i_d \\ i_q \\ i_x \\ i_y \end{bmatrix} + \begin{bmatrix} \psi_f \\ 0 \\ 0 \\ 0 \end{bmatrix} \quad (5)$$

$$T_e = 3n_p(\psi_d i_q - \psi_q i_d) \quad (6)$$

where u_d, u_q and i_d, i_q represent the dq -axes stator voltages and currents, respectively; u_x, u_y and i_x, i_y represent the xy -axes stator voltages and currents, respectively; L_d, L_q , and L_z denote the dq -axes inductances and the leakage inductance, respectively; ψ_s is the stator flux-linkage; θ is the rotor position; T_e is the electromagnetic torque; n_p is the number of pole pairs; and ω is the electric angular velocity.

3. Traditional Direct Torque Control Scheme

The traditional DTC block diagram of DTP-PMSMs is shown in Figure 2 [20,21]. The electromagnetic torque T_e , flux-linkage amplitude $|\psi_s|$, and flux-linkage angle θ_s are obtained through the torque and flux observer on the $\alpha\text{-}\beta$ subspace. The error between the observed value and the given value is transmitted to the hysteresis comparator to obtain the increase and decrease signal of torque flux-linkage.

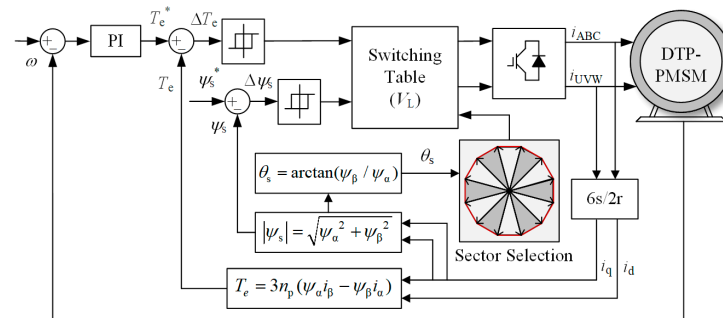


Figure 2. Block diagram of direct torque control for dual three-phase PMSMs.

A DTP-PMSM is driven by a six-phase inverter, where each switching state combination corresponds to a voltage vector in the $\alpha\text{-}\beta$ and $x\text{-}y$ subspaces, with $2^6 = 64$ different spatial voltage vectors, including 4 zero vectors and 60 effective vectors. The voltage vector distribution of the $\alpha\text{-}\beta$ and $x\text{-}y$ subspaces is shown in Figure 3. Numbers of the basic voltage vectors in the figure are, respectively, converted to octal numbers according to the order of bridge arms of ABC and UVW. Effective vectors can be divided into four groups: large vectors, medium-large vectors, medium vectors, and small vectors according to their different amplitudes on the $\alpha\text{-}\beta$ subspace. The amplitudes of voltage vectors of each group are $|V_L| = 0.644U_{dc}$, $|V_{ML}| = 0.471U_{dc}$, $|V_M| = 0.333U_{dc}$, and $|V_S| = 0.173U_{dc}$.

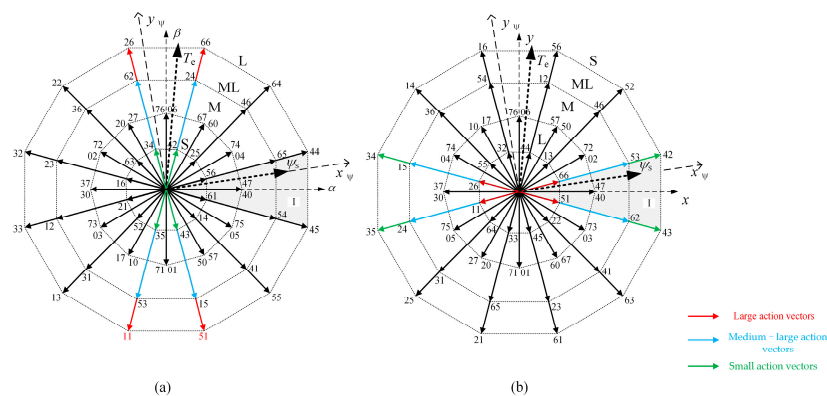


Figure 3. Dual three-phase PMSM voltage vector distribution diagram: (a) $\alpha\text{-}\beta$ subspace; and (b) $x\text{-}y$ subspace.

In order to reduce the complexity of the DTC switching table, the traditional strategy selects the twelve outermost vectors V_L of α - β subspace. Taking the stator flux-linkage in sector I as an example, from the projection of each vector on the flux-linkage axis in Figure 3a, the vectors for torque increase are V_{64} , V_{66} , V_{26} , and V_{22} , where the vectors that have the greatest influence on torque increase are V_{66} and V_{26} . Similarly, the vectors for torque reduction are V_{55} , V_{51} , V_{11} , and V_{13} , where the ones that have the greatest influence on torque reduction are V_{66} and V_{26} . Therefore, according to the fact that the two conditions of the increase and decrease of the torque and the flux-linkage are satisfied at the same time, there will always be an effective vector that is selected in the switching table. Taking sector I as an example, the direct torque switching table for DTP-PMSMs is shown in Table 1.

Table 1. Sector I direct torque control switch table.

Torque Error	Flux-Linkage Error	Voltage Vector
>0	>0	V_{66}
<0	>0	V_{51}
>0	<0	V_{26}
<0	<0	V_{11}

4. Master–Slave Virtual Vector Direct Torque Control Strategy Based on Duty Cycle Allocation

4.1. Virtual Vector Synthesis Method

The traditional DTC strategy only considers the voltage vector effect in the α - β subspace and does not consider the harmonics caused by the vector in the x - y subspace, so there is a large harmonic current. To solve the above problems, two kinds of virtual vector synthesis methods are proposed, which can control the voltage vector amplitude to zero in the harmonic subspace, so as to suppress current harmonics. The two kinds of virtual vectors can make full use of the rich voltage vectors set of DTP-PMSM and can also increase the control accuracy of motor torque under different states because of the different amplitude of the two kinds of virtual vectors.

As shown in Figure 3, V_L , V_{ML} , and V_S have the same direction in the α - β subspace but opposite directions in the x - y subspace. Therefore, the amplitude of the voltage vectors on the harmonic subspace can be controlled to zero by adjusting the action time. Let the action time of V_L , V_{ML} , and V_S be t_1 , t_2 , and t_3 , respectively. The first kind of virtual vector is synthesized via large vectors V_L and medium–large vectors V_{ML} in the same direction and satisfies the following relation:

$$\begin{cases} |\mathbf{V}V_{n\alpha\beta}| = \frac{t_1|V_L|+t_2|V_{ML}|}{T_s} & (n = 1, \dots, 12) \\ |\mathbf{V}V_{nxy}| = \frac{t_1|V_L|-t_2|V_{ML}|}{T_s} = 0 & (n = 1, \dots, 12) \end{cases} \quad (7)$$

The operation time t_1 and t_2 of large and medium–large vectors can be obtained from Equation (6) as follows:

$$\begin{cases} t_1 = 0.73T_s \\ t_2 = 0.27T_s \end{cases} \quad (8)$$

The second kind of virtual vector is synthesized via medium–large vectors V_{ML} and small vectors V_S in the same direction:

$$\begin{cases} |\mathbf{V}V_{n\alpha\beta}| = \frac{t_2|V_{ML}|+t_3|V_S|}{T_s} & (n = 13, \dots, 24) \\ |\mathbf{V}V_{nxy}| = \frac{t_2|V_{ML}|-t_3|V_S|}{T_s} = 0 & (n = 13, \dots, 24) \end{cases} \quad (9)$$

Similarly, the action time t_2 and t_3 of medium–large and small vectors can be solved as follows:

$$\begin{cases} t_2 = 0.58T_s \\ t_3 = 0.42T_s \end{cases} \quad (10)$$

The first kind of virtual vector voltage amplitude is $0.597U_{dc}$, which is very close to the V_L amplitude. Under its action, the motor has larger torque and flux-linkage change, and the dynamic performance is better. The second kind of virtual vector voltage amplitude is $0.345U_{dc}$, about half of the V_L amplitude, which can reduce torque fluctuations and has better steady-state performance, but it is not suitable for larger transient adjustment processes.

In the traditional strategy, regardless of the torque error value, the switching table always outputs a fixed amplitude vector, but this paper chooses the corresponding synthesis method according to the different operating states of the motor. The first kind of virtual vector VV_{1-12} is used in the transient adjustment with a large error, and the second kind of virtual vector VV_{13-24} is used in the steady adjustment with a small error. The distribution of two kinds of virtual vectors in the α - β subspace is shown in Figure 4.

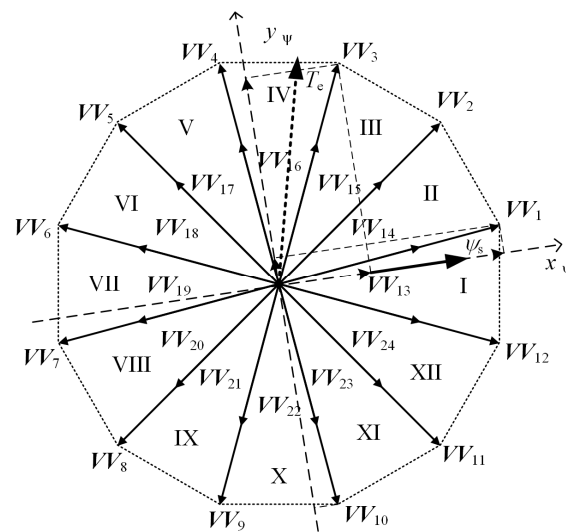


Figure 4. α - β subspace virtual vector distribution.

4.2. Master–Slave Virtual Vector Determination and Duty Cycle Allocation

The two types of virtual vectors of DTP-PMSMs are projected on the stator flux-linkage rotating coordinate system x_ψ - y_ψ , and the torque evaluation function λ_T , flux evaluation function λ_ψ , and back electromotive force evaluation function λ_e are defined as follows [22]:

$$\begin{cases} \lambda_T = \frac{V_{y\psi}}{2/3U_{dc}} \\ \lambda_\psi = \frac{V_{x\psi}}{2/3U_{dc}} \\ \lambda_e = \frac{\omega|\psi_s|}{2/3U_{dc}} \end{cases} \quad (11)$$

where $V_{x\psi}$ and $V_{y\psi}$ are the components of the virtual voltage vector in the stator flux-linkage coordinate system x_ψ -axis and y_ψ -axis, respectively. The flux-linkage position angle θ_s determines the magnitude of the torque and flux-linkage evaluation function, while the back electromotive force evaluation function is related to the electric angular velocity ω .

In order to enhance the torque control effect of DTP-PMSMs, the selection of voltage vectors is no longer limited to only 12 fixed directions. Depending on the sector in which the stator flux is located, the master virtual vector is chosen based on different evaluation functions for each voltage vector, considering its greater influence on torque. The slave virtual vector is selected based on its greater influence on flux-linkage. Both virtual vectors comply with the switching table requirements for torque and flux-linkage increases or decreases; however, their effects differ. Additionally, under different operating states, distinct types of virtual vectors should be selected.

For example, when the stator flux-linkage is in sector I, ΔT_e and $\Delta\psi_s$ are greater than zero. In the transient adjustment of the motor, the evaluation functions corresponding to all virtual vectors are calculated. The first kind of virtual vector VV_{1-3} can increase the flux-linkage as well as the torque. The virtual vector VV_3 with the largest increase in torque is selected as the master virtual vector, and the virtual vector VV_1 with the largest increase in flux-linkage is selected as the slave virtual vector. Similarly, the second kind of virtual vector VV_{15} is selected as the master virtual vector and vector VV_{13} as the slave virtual vector during the steady state adjustment of the motor. According to the above theory, the master–slave virtual vectors satisfying the corresponding conditions can be selected in each sector.

The selected master–slave virtual vectors need to act together in a control period according to a certain duty cycle, and the torque and flux-linkage evaluation function can more accurately represent the degree of influence of the selected master–slave virtual vectors on the torque and flux-linkage of DTP-PMSM. If the duty cycles of the master–slave virtual vectors are d_m and d_s , respectively, the torque change equation in the entire control period is shown as follows:

$$\begin{aligned} \Delta T_e &= \Delta T_{em} + \Delta T_{es} + \Delta T_{e0} \\ &= T_s(\lambda_{Tm}d_m + \lambda_{Ts}d_s - \lambda_e) \end{aligned} \tag{12}$$

$$\frac{\Delta T_e}{L_T} = \lambda_{Tm}d_m + \lambda_{Ts}d_s - \lambda_e \tag{13}$$

where T_s is the control period; ΔT_e is the torque error; L_T is the torque coefficient; and ΔT_{em} , ΔT_{es} , and ΔT_{e0} are the master–slave virtual vector torque changes and the zero vector torque changes, respectively. Similarly, the flux-linkage equation can be expressed as:

$$\frac{\Delta\psi_s}{L_\psi} = \lambda_{\psi m}d_m + \lambda_{\psi s}d_s \tag{14}$$

where $\Delta\psi_s$ is the flux-linkage error; L_ψ is the flux-linkage coefficient; and $\lambda_{\psi m}$ and $\lambda_{\psi s}$ are the flux evaluation functions of master–slave virtual vectors, respectively. The master–slave virtual vector duty cycles d_m and d_s can be calculated by Equations (12) and (13). When the stator flux-linkage is located in sector I, the adjustment range of the master–slave virtual vectors when they act together is shown in Figure 5.

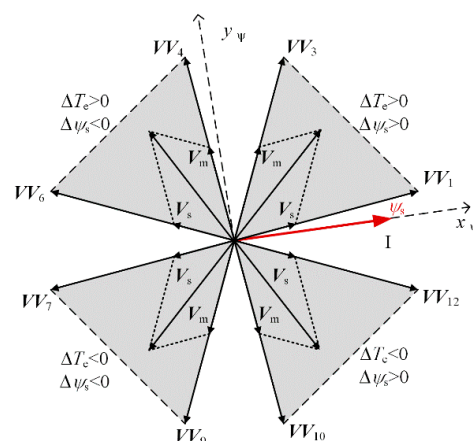


Figure 5. Adjustment range of master–slave virtual vectors.

Due to the large fluctuation of the torque and flux-linkage of DTP-PMSMs, and the imprecision of the torque coefficient and flux-linkage coefficient, the calculated value of the duty cycle of the two virtual vectors may not be between 0 and 1, so it is necessary to

reassign the duty cycle of the master–slave virtual vectors. According to the principle of master virtual vector priority, it can be divided into the following distribution methods:

(1) When d_m and d_s are both less than zero, then the zero vector acts on the whole period;

(2) When d_m is greater than zero or d_s is less than zero, then the main virtual vector acts on the whole period;

(3) When the sum of d_m and d_s is less than 1, the master–slave virtual vectors and zero vector work together on a period;

(4) When d_m is greater than zero and less than 1 and the sum of d_m and d_s is greater than 1, then the master–slave virtual vectors act on a period, where the duty cycle of the slave virtual vector is $1-d_m$.

4.3. Switching Sequence Correction

The switch sequence generated by the synthesis of master–slave virtual vectors in the previous section cannot ensure symmetry, while the constantly changing angle value of θ_s leads to uncertainty in the duty cycles d_m and d_s of master–slave virtual vectors calculated using the evaluation function, further increasing the difficulty in generating a switch sequence. To minimize the disadvantages caused by asymmetric switching sequences, modifications can be made to the switching sequence generated via master–slave virtual vectors based on the output voltage duty cycle relationship for each phase. In the allocation modes mentioned in the previous section, modes (1) and (2) are single-vector actions that do not require modification to the switching sequence. In mode (3), uncertainty exists regarding the relationship between master–slave virtual vector duty cycles, making it difficult to correct the switching sequence. In mode (4), where the sum of the duty cycle for master–slave virtual vectors is 1, their switching sequences across different duty cycle ranges can be corrected through calculation.

Taking the first type of virtual vector acting on the motor in mode (4) as an example, when the stator flux-linkage is located in sector I, VV_3 is the master virtual vector and VV_1 is the slave virtual vector. The phase duty at this time can be calculated using Equation (7), as shown in Table 2. When the duty cycle of phase A and phase B is equal, d_m is 0.73. When the duty cycle of phase V and phase W is equal, d_m is 0.5. Furthermore, when d_m is in different interval ranges, different correction methods can be adopted, as shown in Figure 6. When $0 < d_m \leq 0.27$, the effective vectors V_{44} and V_{65} are replaced by the intermediate vectors V_{04} , V_{64} , and V_{67} to form a symmetric switching sequence. When $0.27 < d_m \leq 0.73$, the effective vectors V_{24} and V_{65} are replaced with the intermediate vectors V_{04} , V_{64} , and V_{67} . When $0.73 < d_m < 1$, the effective vectors V_{24} and V_{66} are replaced with the intermediate vectors V_{04} , V_{64} , and V_{67} . By analogy, the correction methods of switch sequences in different parity sectors can be obtained.

Table 2. Duty cycle of each phase for sectors I and II.

Sector	I	II
Duty cycle of each phase	A $1 - 0.27d_m$	A $1 - 0.73d_m$
	B $0.27 + 0.73d_m$	B $0.73 + 0.27d_m$
	C 0	C 0
	U 1	U $1 - 0.27d_m$
	V $0.73d_m$	V $0.27 + 0.73d_m$
Critical value of d_m	W $0.27 - 0.27d_m$	W 0
	0.27, 0.73	0.5, 0.73

The action time of the high level of each phase of the modified switching sequence does not change, and the modified synthetic vector does not change, which ensures that the effect of the master–slave virtual vector in the two subspaces remains unchanged. Only when the duty cycle of the master–slave virtual vector changes is the individual action vector replaced with the intermediate vector, and each parity sector can be modified to

the symmetric waveform via the equivalent substitution of the intermediate vector within the above three value ranges of d_m . Similarly, the switching sequence of the master–slave virtual vector in synthesis mode 2 can also be modified symmetrically according to this law. The modified master–slave virtual vector switch sequence is symmetrical in the center, which is convenient for hardware implementation, and also ensures that the power device operates once in one period, reducing the switching loss.

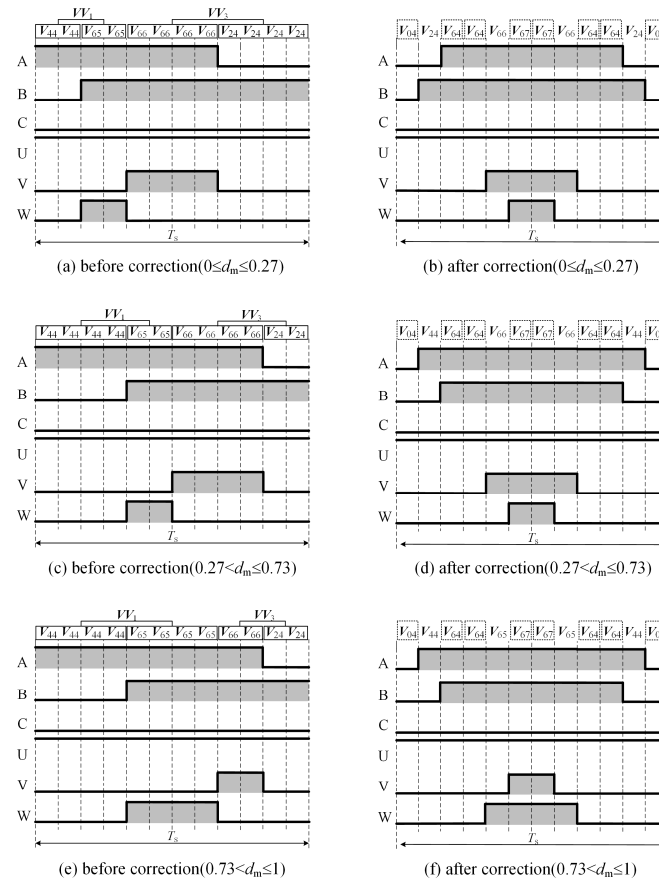


Figure 6. Schematic diagram of switch sequence before and after correction.

The overall block diagram of the master–slave virtual vector DTC of DTP-PMSMs based on duty cycle allocation is shown in Figure 7.

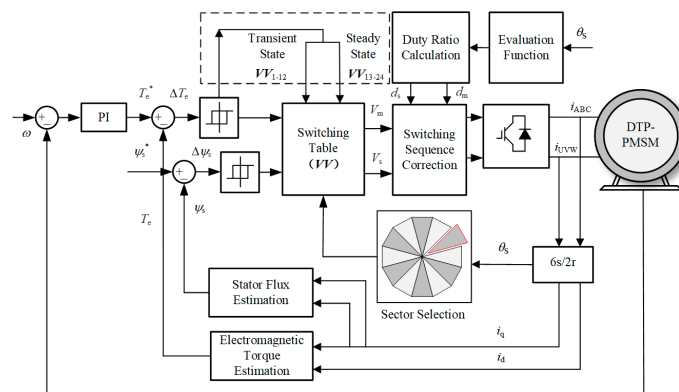


Figure 7. Direct torque control block diagram based on master–slave vector duty cycle allocation.

5. Experimental Verification

5.1. Experiment System

In order to verify the feasibility of the strategy proposed in this paper, a DTP-PMSM system experiment platform is built, as shown in Figure 8. The rated speed of the dual three-phase permanent magnet synchronous motor, which is manufactured by Hebei Electric Machinery Factory in China, used in the experiment is 1000 r/min, the rated torque is 10 Nm, the permanent magnet flux is 0.22 Wb, the pole-pairs number is 5, the d-axis inductance is 29 mH, and the q-axis inductance is 42 mH, respectively. The control algorithm is implemented with the TMS320F28377D DSP produced by TI, and Cyclone V FPGA produced by Intel. DSP is applied to execute the algorithm, and FPGA is applied to implement the high-precision analog-to-digital conversion (ADC) sampling, digital-to-analog conversion (DAC) conversion, and PWM pulse generation. The switching frequency of the IPM is 10 kHz.

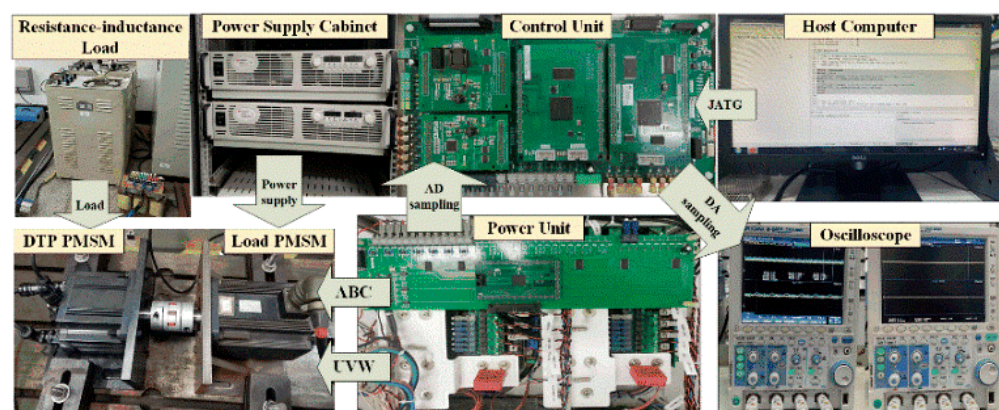
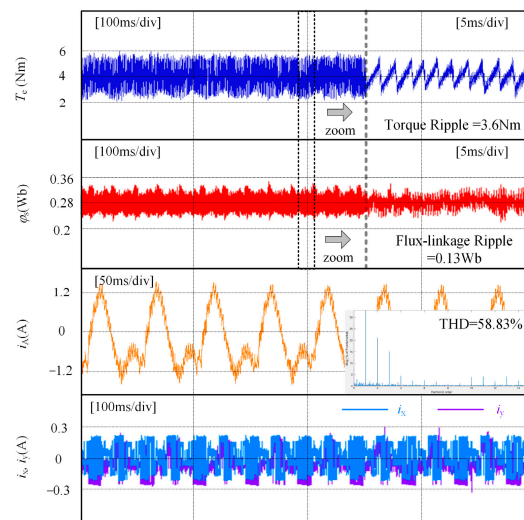


Figure 8. Experimental platform for the DTP-PMSM control system.

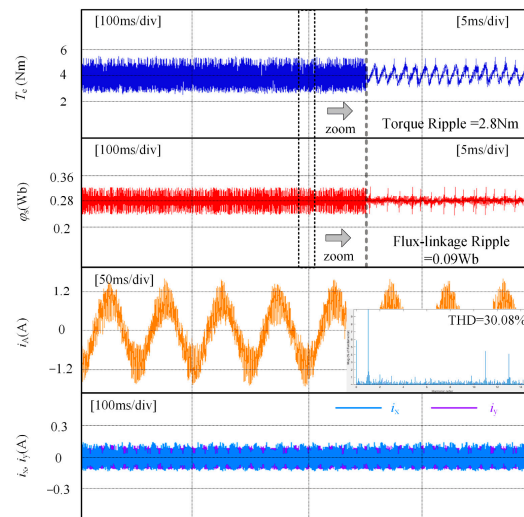
The experimental platform consists of a power loop in the strong electricity part and a control loop in the weak electricity part. After the experimental platform is powered on and debugged, Code Composer Studio (ccs10.0) is used to build the DSP experimental program. The experiment simulates the variable load of the motor through the series inductance of the resistance box. In the strong electricity part of the experimental platform, the DC bus voltage of the system is powered with the KEYSIGHT DC power supply. In the pulse transmission process of the system, the duty cycle signal is first sent from the main control panel to the CPLD panel. In the CPLD, the signal is converted into an optical signal through the optocoupler module, and then the 12-channel PWM wave is sent to the IPM through the optical fiber. The reference voltage is synthesized by controlling the opening and closing of the IGBT switch tube in the IPM module. The control loop of the weak electricity part of the experimental platform is composed of the DSP chip and the FPGA chip. The DSP chip mainly performs the operation of the basic algorithm of the motor. The DSP converts the algorithm into a duty cycle and controls the FPGA chip to generate a pulse signal. The pulse signal is transmitted to the CPLD board to generate a 12-channel PWM wave and is converted into the optical signal to control the opening and closing of the IPM.

5.2. Analysis of Steady-State Experimental Results

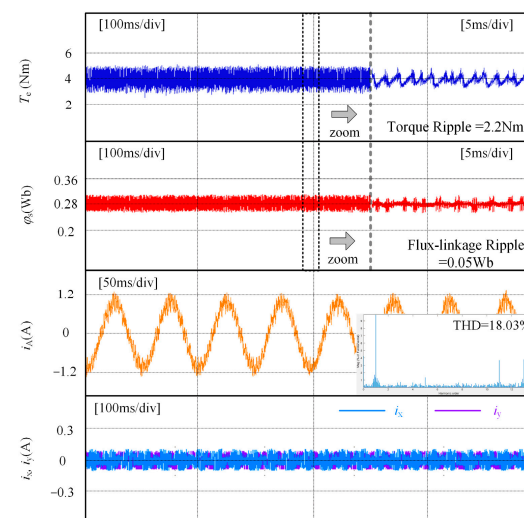
To verify the steady-state performance of the proposed strategy, the motor runs at 300 r/min with a load of 4 Nm. After steady-state operation, the experimental waveforms of the traditional strategy, the virtual vector strategy, and the proposed strategy are shown in Figure 9.



(a)



(b)



(c)

Figure 9. Steady-state operation experimental waveforms: (a) traditional strategy; (b) virtual vector strategy; and (c) proposed strategy.

By referring to the literature on DTC strategy in recent years, most of the improved DTC strategies are mainly analyzed from the three perspectives of the harmonic content analysis of motor current, torque ripple, and flux-linkage ripple. The traditional DTC strategy does not consider the voltage vector synthesis of the harmonic subspace, but the proposed control strategy can suppress the voltage synthesis of the harmonic subspace by redistributing the vector operation time. By analyzing the experimental results in Figure 9, under steady-state conditions, the phase current THD of the traditional DTC strategy is 58.8%, the torque ripple is 3.6 Nm, and the flux-linkage ripple is 0.13 Wb. However, the phase current THD of the proposed strategy is 18.0%, the torque ripple is 2.2 Nm, and the flux-linkage ripple is 0.05 Wb. Compared with the traditional DTC control strategy, the current THD of the proposed strategy is reduced by 69.4%, the torque ripple is reduced by 39%, and the flux-linkage ripple is reduced by 62%, which verifies the effectiveness of the proposed control strategy. Moreover, the experimental analysis results show that the proposed control strategy can effectively suppress the harmonic subspace current i_x, i_y . By analyzing the basic mathematical Equations (3)–(6) of the motor, it can be concluded that the harmonic subspace current will affect the flux-linkage of the harmonic subspace, which will adversely affect the flux-linkage φ_s of the motor.

In addition, by analyzing other works in the literature [23], in order to further analyze the improvement effect of the proposed control strategy on motor flux-linkage and torque, two new variables are introduced: the torque standard deviation σ_{T_e} and the flux-linkage standard deviation σ_{φ_s} . By introducing these two new evaluation variables, the effect of the proposed control strategy is further verified. After the analysis, it can be obtained that σ_{T_e} is reduced by 43% and σ_{φ_s} is reduced by 27% compared with the traditional control strategy under 300 r/min with a load of 4 Nm condition.

In order to further verify the steady-state performance of the proposed strategy under different conditions, the phase current THD, torque ripple values, and flux-linkage ripple values of the three control strategies under different load values are shown in Table 3 at the reference speed of 300 r/min.

Table 3. Steady-state performance comparison under different load conditions.

Control Strategy		4 Nm	6 Nm	8 Nm
Current THD (%)	a	58.8	42.7	36.5
	b	30.1	24.6	20.8
	c	18.0	16.2	14.8
Torque Ripple (Nm)	a	3.6	4.5	5.3
	b	2.8	3.7	4.2
	c	2.2	3.3	3.6
Flux-linkage Ripple (Wb)	a	0.13	0.14	0.16
	b	0.09	0.11	0.14
	c	0.05	0.06	0.08

From Table 3, it is obvious that compared to the traditional DTC strategy and virtual vector strategy, the strategy proposed in this paper reduces flux-linkage fluctuation and torque fluctuation under various conditions. After using two sets of virtual vectors, the phase current waveform is greatly improved.

5.3. Analysis of Dynamic Experimental Results

As shown in Figures 10 and 11, so as to verify the dynamic tracking performance of the proposed strategy, an experimental analysis was carried out under three different working conditions: the reference speed in the first working condition jumped from 300 r/min to 500 r/min and the second condition is that the motor is suddenly loaded by 4 Nm during no-load time until stable operation.

From Figure 10, it is obvious that the two control strategies can quickly track the reference value of the speed after the motor is started, there is no large overshoot phenomenon,

and the speed of the proposed control strategy reaches the given reference value after a short adjustment when the speed changes at different speeds. It can be seen that the proposed strategy has good speed dynamic control performance.

As can be seen from Figure 11, both control strategies quickly reach the same torque value after the abrupt addition of a 4 Nm load. Therefore, the proposed strategy retains the advantages of the traditional strategy of fast response, and the proposed strategy can effectively suppress the torque fluctuation and flux-linkage fluctuation of DTP-PMSMs.

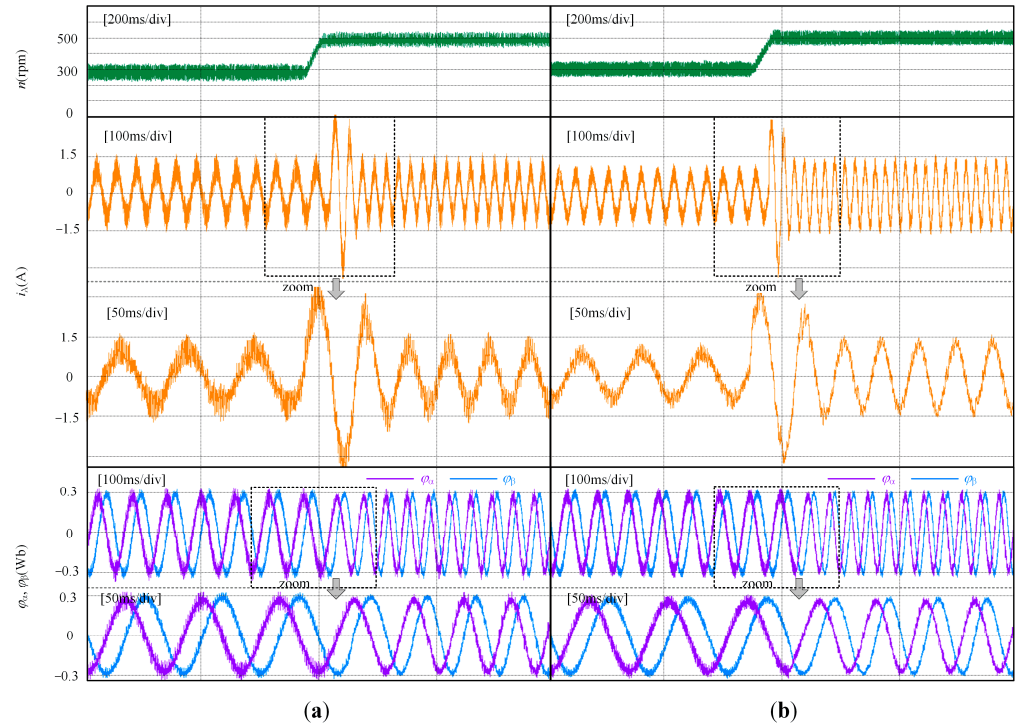


Figure 10. Experimental waveform of step speed response: (a) virtual vector strategy; (b) proposed strategy.

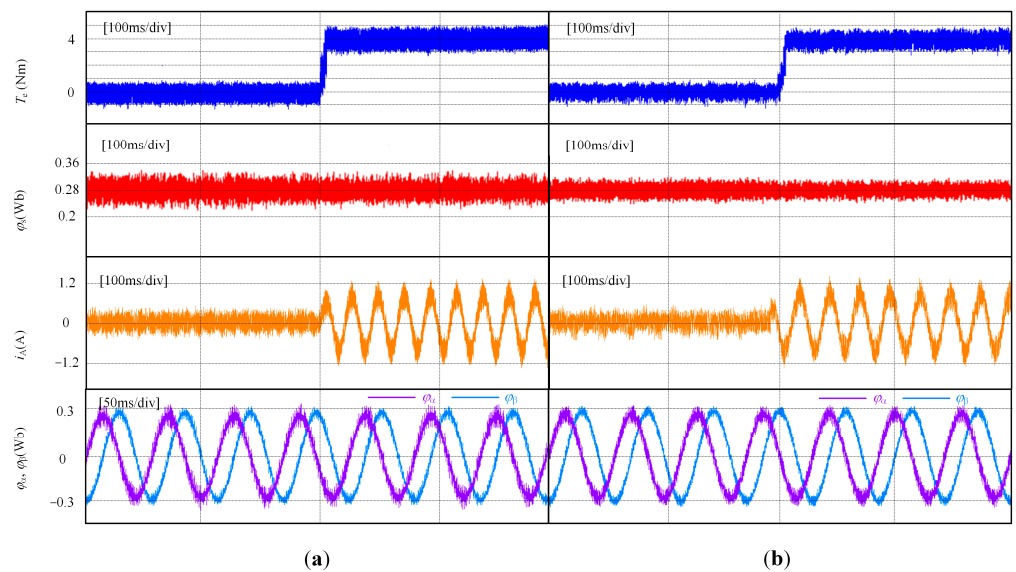


Figure 11. Load dynamic experimental waveform: (a) virtual vector strategy; (b) proposed strategy.

6. Conclusions

In this paper, a DTC strategy combining master–slave virtual vector duty cycle allocation is proposed for a DTP-PMSM system. Through experimental verification, the conclusions are as follows:

- (1) The use of virtual vectors reduces the voltage amplitude of the x - y subspace to zero, effectively reducing the 5th and 7th harmonics, and also uses two types of virtual vectors to increase the torque control accuracy;
- (2) Using the exact value of the evaluation function to calculate and assign the duty cycle of the master–slave virtual vector, the torque fluctuation and flux-linkage fluctuation are reduced, and the adjustment range of the vector is increased;
- (3) The switching sequence of the master–slave virtual vector is remodified, and the effective vector action sequence under different sectors and different duty cycle values is analyzed, which reduces the difficulty of hardware implementation and ensures the effectiveness of harmonic suppression.

Author Contributions: Conceptualization, Q.G.; Data Curation, Z.Q.; Formal Analysis, G.Z.; Funding Acquisition, Z.Z. and Q.G.; Investigation, X.J.; Methodology, Z.Z.; Project Administration, Q.G.; Resources, Q.G.; Software, X.J.; Supervision, G.Z. and Q.G.; Validation, X.J.; Visualization, Z.Q.; Writing—Original Draft, Z.Q. All authors have read and agreed to the published version of the manuscript.

Funding: This research was supported in part by the National Natural Science Foundation of China under Grant 52077154, in part by the Natural Science Foundation of the Tianjin Municipality under Grant 23JCYBJC00290, and in part by the Zhejiang Provincial Natural Science Foundation of China under Grant LY24E070003.

Institutional Review Board Statement: Not applicable.

Informed Consent Statement: Not applicable.

Data Availability Statement: The original contributions presented in the study are included in the article, further inquiries can be directed to the corresponding author.

Conflicts of Interest: The authors declare no conflicts of interest.

References

1. Hu, Y.; Zhu, Z.; Odavic, M. Comparison of Two-Individual Current Control and Vector Space Decomposition Control for Dual Three-Phase PMSM. *IEEE Trans. Ind. Appl.* **2017**, *53*, 4483–4492. [[CrossRef](#)]
2. Kallio, S.; Andriollo, M.; Tortella, A.; Karttunen, J. Decoupled d-q Model of Double-Star Interior-Permanent-Magnet Synchronous Machines. *IEEE Trans. Ind. Electron.* **2013**, *60*, 2486–2494. [[CrossRef](#)]
3. Huang, L.; Ji, J.; Zhao, W.; Tang, H.; Tao, T.; Jin, S. Direct torque control for dual three-phase permanent magnet motor with improved torque and flux. *IEEE Trans. Energy Convers.* **2022**, *37*, 2385–2397. [[CrossRef](#)]
4. Zhao, Y.; Lipo, T.A. Space vector PWM control of dual three-phase induction machine using vector space decomposition. *IEEE Trans Ind. Appl.* **1995**, *31*, 1100–1109. [[CrossRef](#)]
5. Demir, Y.; Aydin, M. A Novel Dual Three-Phase Permanent Magnet Synchronous Motor with Asymmetric Stator Winding. *IEEE Trans. Magn.* **2016**, *52*, 1–5. [[CrossRef](#)]
6. Huang, L.; Ji, J.; Zhao, W.; Tao, T.; Cui, J. Duty-ratio-based direct torque control with enhanced harmonic current suppression for dual-three-phase permanent magnet motor. *IEEE Trans. Power Electron.* **2022**, *37*, 11098–11108. [[CrossRef](#)]
7. Gonzalez-Prieto, I.; Duran, M.J.; Aciego, J.J.; Martin, C.; Barrero, F. Model Predictive Control of Six-Phase Induction Motor Drives Using Virtual Voltage Vectors. *IEEE Trans. Ind. Electron.* **2018**, *65*, 27–37. [[CrossRef](#)]
8. Xu, J.; Odavic, M.; Zhu, Z.; Wu, Z.; Nuno, F. Switching-table-based direct torque control of dual three-phase PMSMs with closed-loop current harmonics compensation. *IEEE Trans. Power Electron.* **2021**, *36*, 10645–10659. [[CrossRef](#)]
9. Ren, Y.; Zhu, Z. Enhancement of Steady-State Performance in Direct-Torque-Controlled Dual Three-Phase Permanent-Magnet Synchronous Machine Drives with Modified Switching Table. *IEEE Trans. Ind. Electron.* **2015**, *62*, 3338–3350. [[CrossRef](#)]
10. Shao, B.; Zhu, Z.; Feng, J.; Guo, S.; Li, Y.; Liao, W. Compensation of Selective Current Harmonics for Switching-Table-Based Direct Torque Control of Dual Three-Phase PMSM Drives. *IEEE Trans. Ind. Appl.* **2021**, *57*, 2505–2515. [[CrossRef](#)]
11. Ren, Y.; Zhu, Z.; Green, J.E.; Li, Y.; Zhu, S.; Li, Z. Improved Duty-Ratio-Based Direct Torque Control for Dual Three-Phase Permanent Magnet Synchronous Machine Drives. *IEEE Trans. Ind. Appl.* **2019**, *55*, 5843–5853. [[CrossRef](#)]

12. Ren, Y.; Zhu, Z. Reduction of Both Harmonic Current and Torque Ripple for Dual Three-Phase Permanent-Magnet Synchronous Machine Using Modified Switching-Table-Based Direct Torque Control. *IEEE Trans. Ind. Electron.* **2015**, *62*, 6671–6683. [[CrossRef](#)]
13. Li, L.; Zhu, G. Electromagnetic-thermal-stress efforts of stator-casing grease buffers for permanent magnet driving motors. *IEEE Trans. Ind. Appl.* **2023**, *60*, 1268–1276. [[CrossRef](#)]
14. Wang, X.; Wang, Z.; Xu, Z. A Hybrid Direct Torque Control Scheme for Dual Three-Phase PMSM Drives with Improved Operation Performance. *IEEE Trans. Power Electron.* **2019**, *34*, 1622–1634. [[CrossRef](#)]
15. Luo, Y.; Liu, C. Model Predictive Control for a Six-Phase PMSM With High Robustness Against Weighting Factor Variation. *IEEE Trans. Ind. Appl.* **2019**, *55*, 2781–2791. [[CrossRef](#)]
16. Luo, Y.; Liu, C. A Flux Constrained Predictive Control for a Six-Phase PMSM Motor with Lower Complexity. *IEEE Trans. Ind. Electron.* **2019**, *66*, 5081–5093. [[CrossRef](#)]
17. Luo, Y.; Liu, C. A Simplified Model Predictive Control for a Dual Three-Phase PMSM With Reduced Harmonic Currents. *IEEE Trans. Ind. Electron.* **2018**, *65*, 9079–9089. [[CrossRef](#)]
18. Deng, W.; Zhang, X.; Yan, B. An Enhanced Discrete Virtual Vector-Based Direct Torque Control of PMSM Drives. *IEEE Trans. Energy Convers.* **2024**, *39*, 277–286. [[CrossRef](#)]
19. Liu, Y.; Lyu, M.; Huang, S.; Liao, W.; Huang, S. Direct Torque Control Schemes for Dual Three-Phase PMSM Considering Unbalanced DC-link Voltages. *IEEE Trans. Energy Convers.* **2024**, *39*, 229–242. [[CrossRef](#)]
20. Qiu, X.; Ji, J.; Zhou, D.; Zhao, W.; Chen, Y.; Huang, L. A modified flux observer for sensorless direct torque control of dual three-phase PMSM considering open-circuit fault. *IEEE Trans. Power Electron.* **2022**, *37*, 15356–15369. [[CrossRef](#)]
21. Xia, C.; Zhao, J.; Yan, Y.; Shi, T. A Novel Direct Torque and Flux Control Method of Matrix Converter-Fed PMSM Drives. *IEEE Trans. Power Electron.* **2014**, *29*, 5417–5430. [[CrossRef](#)]
22. Xia, C.; Zhao, J.; Yan, Y.; Shi, T. A Novel Direct Torque Control of Matrix Converter-Fed PMSM Drives Using Duty Cycle Control for Torque Ripple Reduction. *IEEE Trans. Ind. Electron.* **2014**, *61*, 2700–2713. [[CrossRef](#)]
23. Shao, B.; Zhu, Z.; Yan, L.; Feng, J.; Guo, S.; Li, Y.; Ling, F. Torque ripple reduction for direct torque control of dual three-phase PMSM based on multiple virtual voltage vectors. *IEEE Trans. Energy Convers.* **2022**, *38*, 296–309. [[CrossRef](#)]

Disclaimer/Publisher’s Note: The statements, opinions and data contained in all publications are solely those of the individual author(s) and contributor(s) and not of MDPI and/or the editor(s). MDPI and/or the editor(s) disclaim responsibility for any injury to people or property resulting from any ideas, methods, instructions or products referred to in the content.